Supplementary Material

Uncertainty-aware modelling of climate-driven transmission suitability for cutaneous leishmaniasis in North Africa

Supplementary Material A: Next generation matrix

Specifically, we define the state vector for the four-stage population model as:

$$\mathrm{n} = \begin{bmatrix} E \\ L \\ N \\ A \end{bmatrix}$$

The system dynamics are given by:

$$\frac{dE}{dt} = FA - (D_1 + M_1)E \quad (1)$$

$$\frac{dL}{dt} = D_1E - (D_2 + M_2)L \quad (2)$$

$$\frac{dN}{dt} = D_2L - (D_3 + M_3)N \quad (3)$$

$$\frac{dA}{dt} = D_3N - M_4A \quad (4)$$

Derivation of the basic reproduction number R_0

Decomposition into new recruitment and transitions

We decompose the right-hand side of the ODE system into two parts:

- $\mathcal{F}$: The rate of appearance of new recruitment (i.e., entry into the first compartment, eggs, via reproduction).
- $\mathcal{V}$: The rate of transfer of individuals between compartments (development) minus the rate of removal (mortality).

For our model:

$$\frac{d\mathbf{n}}{dt} = \mathcal{F} - \mathcal{V} \quad (5)$$

$$\mathcal{F} = \begin{bmatrix} FA \\ 0 \\ 0 \\ 0 \end{bmatrix}, \mathcal{V} = \begin{bmatrix} (D_1 + M_1)E \\ -D_1E + (D_2 + M_2)L \\ -D_2L + (D_3 + M_3)N \\ -D_3N + (F + M_4)A \end{bmatrix} \quad (6)$$

The next-generation matrix $\boldsymbol{FV^{-1}}$

The matrices F and V are defined as the Jacobians of $\mathcal{F}$ and $\mathcal{V}$ with respect to the state vector n, evaluated at the disease-free equilibrium ($\mathrm{n}^* = 0$):

$$F = \begin{bmatrix} \frac{\partial \mathcal{F}_1}{\partial F} & \frac{\partial \mathcal{F}_1}{\partial \mathcal{F}_2} & \frac{\partial \mathcal{F}_1}{\partial N} & \frac{\partial \mathcal{F}_1}{\partial A} \\ \frac{\partial \mathcal{F}_2}{\partial F} & \frac{\partial \mathcal{F}_2}{\partial \mathcal{F}_3} & \frac{\partial \mathcal{F}_2}{\partial N} & \frac{\partial \mathcal{F}_2}{\partial A} \\ \frac{\partial \mathcal{F}_3}{\partial F} & \frac{\partial \mathcal{F}_3}{\partial \mathcal{F}_4} & \frac{\partial \mathcal{F}_3}{\partial N} & \frac{\partial \mathcal{F}_3}{\partial \mathcal{A}} \\ \frac{\partial \mathcal{F}_4}{\partial E} & \frac{\partial \mathcal{F}_4}{\partial L} & \frac{\partial \mathcal{F}_4}{\partial N} & \frac{\partial \mathcal{F}_4}{\partial A} \end{bmatrix}_{\mathbf{n}^*} = \begin{bmatrix} 0 & 0 & 0 & F \\ 0 & 0 & 0 & 0 \\ 0 & 0 & 0 & 0 \\ 0 & 0 & 0 & 0 \end{bmatrix} (7)$$

$$V = \begin{bmatrix} \frac{\partial \mathcal{V}_1}{\partial F} & \frac{\partial \mathcal{V}_1}{\partial L} & \frac{\partial \mathcal{V}_1}{\partial N} & \frac{\partial \mathcal{V}_1}{\partial \mathcal{A}} \\ \frac{\partial \mathcal{V}_2}{\partial F} & \frac{\partial \mathcal{V}_2}{\partial L} & \frac{\partial \mathcal{V}_2}{\partial N} & \frac{\partial \mathcal{V}_2}{\partial A} \\ \frac{\partial \mathcal{V}_3}{\partial F} & \frac{\partial \mathcal{V}_3}{\partial L} & \frac{\partial \mathcal{V}_3}{\partial N} & \frac{\partial \mathcal{V}_3}{\partial A} \\ \frac{\partial \mathcal{V}_4}{\partial E} & \frac{\partial \mathcal{V}_4}{\partial L} & \frac{\partial \mathcal{V}_4}{\partial N} & \frac{\partial \mathcal{V}_4}{\partial A} \end{bmatrix}_{\mathbf{n}^*} = \begin{bmatrix} D_1 + M_1 & 0 & 0 & 0 \\ -D_1 & D_2 + M_2 & 0 & 0 \\ 0 & -D_2 & D_3 + M_3 & 0 \\ 0 & 0 & -D_3 & F + M_4 \end{bmatrix} (8)$$

Detailed inversion of the matrix V

The matrix V is invertible. Its inverse V^{-1} is found by solving $V \cdot V^{-1} = I$. Given V is lower triangular, V^{-1} is also lower triangular. Let us denote the unknown inverse as:

$$V^{-1} = \begin{bmatrix} a & 0 & 0 & 0 \\ b & c & 0 & 0 \\ d & e & f & 0 \\ g & h & i & j \end{bmatrix} (9)$$

We perform the multiplication $V \cdot V^{-1}$ and set it equal to I, solving for each element step-by-step.

Row 1 of V × columns of V^{-1}

$$\text{Row 1: } [D_1 + M_1 \quad 0 \quad 0 \quad 0]$$

$$\text{Col 1: } (D_1 + M_1)a = 1 \Rightarrow a = \frac{1}{D_1 + M_1}$$

Col 2-4: All yield 0, which matches I.

Row 2 of V × Columns of V^{-1}

$$\text{Row 2: } -D_1 \quad D_2 + M_2 \quad 0 \quad 0]$$

$$\text{Col 1: } -D_1 a + (D_2 + M_2)b = 0 \Rightarrow (D_2 + M_2)b = D_1 a$$
$$\Rightarrow b = \frac{D_1}{(D_1 + M_1)(D_2 + M_2)}$$

$$\text{Col 2: } (D_2 + M_2)c = 1 \Rightarrow c = \frac{1}{D_2 + M_2}$$

Col 3-4: yield 0, matching I.

Row 3 of V × columns of V^{-1}

$$\text{Row 3: } [0 \quad -D_2 \quad D_3 + M_3 \quad 0]$$

$$\text{Col 1: } -D_2 b + (D_3 + M_3)d = 0 \Rightarrow (D_3 + M_3)d = D_2 b$$
$$\Rightarrow d = \frac{D_1 D_2}{(D_1 + M_1)(D_2 + M_2)(D_3 + M_3)}$$

$$\text{Col 2: } -D_2c + (D_3 + M_3)e = 0 \Rightarrow (D_3 + M_3)e = D_2c$$
$$\Rightarrow e = \frac{D_2}{(D_2 + M_2)(D_3 + M_3)}$$

$$\text{Col 3: } (D_3 + M_3)f = 1 \Rightarrow f = \frac{1}{D_3 + M_3}$$

Col 4: yields 0, matching I.

Row 4 of V × columns of V^{-1}

$$\text{Row 4: } [0 \quad 0 \quad -D_3 \quad F + M_4]$$

$$\text{Col 1: } -D_3d + M_4g = 0 \Rightarrow M_4g = D_3d$$
$$\Rightarrow g = \frac{D_1D_2D_3}{(D_1 + M_1)(D_2 + M_2)(D_3 + M_3)M_4}$$

$$\text{Col 2: } -D_3e + M_4h = 0 \Rightarrow M_4h = D_3e$$
$$\Rightarrow h = \frac{D_2D_3}{(D_2 + M_2)(D_3 + M_3)M_4}$$

$$\text{Col 3: } -D_3f + M_4i = 0 \Rightarrow M_4i = D_3f$$
$$\Rightarrow i = \frac{D_3}{(D_3 + M_3)M_4}$$

$$\text{Col 4: } M_4j = 1 \Rightarrow j = \frac{1}{M_4}$$

Final result for V^{-1}

Assembling all elements, the inverse matrix is:

$$V^{-1} = \begin{bmatrix} \frac{1}{D_1+M_1} & 0 & 0 & 0 \\ \frac{D_1}{(D_1+M_1)(D_2+M_2)} & \frac{1}{D_2+M_2} & 0 & 0 \\ \frac{D_1D_2}{(D_1+M_1)(D_2+M_2)(D_3+M_3)} & \frac{D_1D_2D_3}{(D_2+M_2)(D_3+M_3)} & \frac{1}{D_3+M_3} & 0 \\ \frac{D_2D_3}{(D_1+M_1)(D_2+M_2)(D_3+M_3)M_4} & \frac{D_3}{(D_2+M_2)(D_3+M_3)M_4} & \frac{D_3}{(D_3+M_3)M_4} & \frac{1}{M_4} \end{bmatrix} \quad (10)$$

Biological interpretation of V^{-1}

The matrix V^{-1} is the fundamental matrix of the linear system. Its elements have an underlying biological meaning: the element $(V^{-1})_{ij}$ represents the expected total time an individual originating in compartment j will spend in compartment i over its lifetime, before dying or exiting the system. For example:

- $(V^{-1})_{11} = \frac{1}{D_1+M_1}$: average time an egg spends in the egg stage.
- $(V^{-1})_{41} = g$: expected time a newly hatched egg will spend as an adult.
- $(V^{-1})_{44} = \frac{1}{F+M_4}$: average lifespan of an adult.

Definition of R_0

The next-generation matrix is $K = FV^{-1}$. Since F has only one non-zero row, K is a rank- 1 matrix:

$$K = FV^{-1} = \begin{bmatrix} 0 & 0 & 0 & F \\ 0 & 0 & 0 & 0 \\ 0 & 0 & 0 & 0 \\ 0 & 0 & 0 & 0 \end{bmatrix} \cdot V^{-1} = \begin{bmatrix} F \cdot g & F \cdot h & F \cdot i & F \cdot j \\ 0 & 0 & 0 & 0 \\ 0 & 0 & 0 & 0 \\ 0 & 0 & 0 & 0 \end{bmatrix} \quad (11)$$

R_0 is the spectral radius (dominant eigenvalue) of K. For this rank- 1 matrix, the only non-zero eigenvalue is its trace, which is $K_{11} = F \cdot g$. Therefore:

$$R_0 = F \cdot g = \frac{F \cdot D_1 \cdot D_2 \cdot D_3}{(D_1+M_1)(D_2+M_2)(D_3+M_3)M_4} \quad (12)$$

R_0 derived from the next-generation matrix method, has a direct biographic interpretation: the average number of offspring an individual produces over its lifetime. The threshold $R_0 = 1$ signifies the point where each generation replaces itself.

Supplementary Material B: Daily biting rate of *Phlebotomus papatasi*

To parameterize the daily biting rate of *Phlebotomus papatasi*, we used empirical data from controlled laboratory experiments in which groups of five female sand flies were observed for biting behavior over 30- and 90-minute intervals (Parkash et al., 2021). According to Table 2 of the study, the mean number of bites per five flies during 30-minute exposure yielded a per-fly biting rate, which we extrapolated to a 2-hour crepuscular window to reflect typical evening biting activity. Since *P. papatasi* completes one gonotrophic cycle approximately every 6 days under moderate temperatures (23–26 °C), the resulting estimate was averaged over this cycle length to obtain a realistic daily biting rate. Incorporating the observed standard deviation, we derived an estimated biting rate of 0.19 ± 0.08 bites per fly per day, corresponding to a plausible range of 0.11 to 0.27. This estimate aligns with field-based observations for *Phlebotomus* species and was adopted as a fixed parameter in our vectorial capacity model, with the associated uncertainty retained for sensitivity analysis.

Estimation of Extrinsic Incubation Period (EIP) for Leishmania major in Phlebotomus papatasi

Direct empirical measurements of the extrinsic incubation period (EIP) in *Phlebotomus papatasi* are limited. However, informed approximations can be made using studies from closely related vectors and temperature-dependent infection outcomes. Lawyer et al. 1990) documented that in *Phlebotomus duboscqi*, a competent vector within the same subgenus (*Phlebotomus*, subgenus *Phlebotomus*), metacyclic promastigotes—the infective form of *Leishmania major*—first appeared approximately six days post-bloodmeal at 23 °C. Although *P. duboscqi* is not identical to *P. papatasi*, both species share similar ecological roles and midgut physiology, making this observation a reasonable biological proxy. This inference is further supported by Benkova and Volf (2007), who observed significantly higher infection intensities and successful parasite maturation in *P. papatasi* reared at 23 °C compared to 28 °C. These findings indicate that cooler temperatures favor prolonged digestion and allow sufficient time for *L. major* to complete its development.

To estimate EIP at higher temperatures, we used the known principle that parasite development accelerates with temperature until an optimum is surpassed—consistent with enzymatic reaction rates and vector physiology. Since EIP is inversely related to temperature-driven developmental speed, we applied a biologically informed monotonic decay: shorter EIP at warmer temperatures, but also incorporating empirical observations of declining infection success. Specifically, we conservatively set EIP to ~7 days at 23 °C (as observed in *P. duboscqi*), then inferred ~6.5 days at 26 °C and ~5 days at 28 °C, consistent with qualitative infection outcomes and accelerated digestion noted in *P. papatasi* at those temperatures (Benkova & Volf, 2007). To represent the temperature dependence of EIP, we fitted these values using an exponential decay model, which offered a biologically plausible approximation of the observed trend. These temperature-scaled estimates were then used to parameterize the vectorial capacity model.

Supplementary Material C: Ecological niche of rodent under the present and future scenarios

Present and future Global-AI layers were obtained from Version 3 of the Global Aridity Index and Potential Evapotranspiration Database (Global-AI_PET_v3) at 30-arc-second resolution for the 1970–2000 climatological period. These variables quantify long-term atmospheric water demand and rainfall deficit based on the FAO-56 Penman–Monteith formulation retrieved from https://doi.org/10.6084/m9.figshare.20088368 (Zomer et al.,

2022) and provide an ecophysiologically meaningful representation of aridity constraints on small-mammal habitats. Monthly NDVI data (February 2000–November 2025) were acquired from the MODIS MOD13A2 Collection 6.1 product at 1-km resolution via Google Earth Engine and aggregated into long-term monthly (climatologies https://developers.google.com/earth-engine/datasets/catalog/MODIS_061_MOD13A2#bands) (Didan, 2021). Soil data was retrieved from https://data.isric.org/geonetwork/srv/eng/catalog.search#/metadata/4727602b-d0f2-4a6d-bb2f-d50c0ee24298 (Hengl et al., 2015).

All data were retrieved on 2 January 2026.

Occurrence data

Species occurrence records were compiled as presence-only observations with geographic coordinates. Longitude and latitude fields were automatically identified and standardized, and all records were projected to the WGS84 geographic coordinate reference system. Occurrences were encoded as binary presences (presence = 1) and used to construct spatial point objects for modelling.

Environmental predictors

Environmental predictors were provided as raster layers and harmonized prior to modelling. All rasters were reprojected (where necessary), cropped, and resampled to match a single reference raster using bilinear interpolation, ensuring consistent spatial resolution and extent. Predictor values were extracted at occurrence locations, and variables with zero variance across occurrences were excluded.

Collinearity assessment and predictor selection

Pairwise correlations among extracted predictor values were computed and visualized using correlation matrices and hierarchical clustering based on dissimilarity (1 − r). These diagnostics were used for exploratory assessment of collinearity. Final predictor selection was performed manually by retaining a subset of predictors deemed ecologically interpretable and numerically stable for model fitting.

Background sampling

Pseudo-absence (background) points were generated using a geographically constrained distance-based method (gDist). For each presence location, 10 background points were sampled, resulting in a background-to-presence ratio of 10:1.

Model fitting

Species distribution models were fitted using an ensemble framework implemented in the sdm package (Naimi & Araújo, 2016). Three modelling algorithms were applied: generalized linear models (GLM), generalized additive models (GAM), and random forests (RF). Model calibration employed 5-fold cross-validation, repeated three times using independent random partitions. Model fitting was parallelized across four CPU cores.

Model evaluation

Model performance was evaluated using discrimination metrics calculated internally by the sdm framework, including the area under the receiver operating characteristic curve (AUC) and the true skill statistic (TSS). Evaluation metrics were recorded for all cross-validation folds and repetitions.

Ensemble modelling and present-day prediction

Ensemble predictions were generated by combining individual model outputs using both simple averaging and performance-weighted averaging, with weights derived from AUC and TSS scores. The resulting ensemble surface represents present-day habitat suitability on a continuous scale.

Future projections

The trained ensemble model was projected onto mid-century (circa 2050) environmental conditions under two scenarios (SSP2-4.5 and SSP5-8.5). Future raster layers were processed using the same reprojection, cropping, and resampling procedures applied to present-day predictors. Only predictors retained during model training were used in future projections.

The ensemble SDM exhibited very high predictive skill, with an AUC of 0.996 and a prevalence-adjusted accuracy of 0.982, indicating excellent discrimination between suitable and unsuitable areas. Model predictions were strongly correlated with observed occurrences (Pearson $r = 0.76$, $p < 10^{-104}$) and showed low deviance (0.07), confirming robust overall model fit.

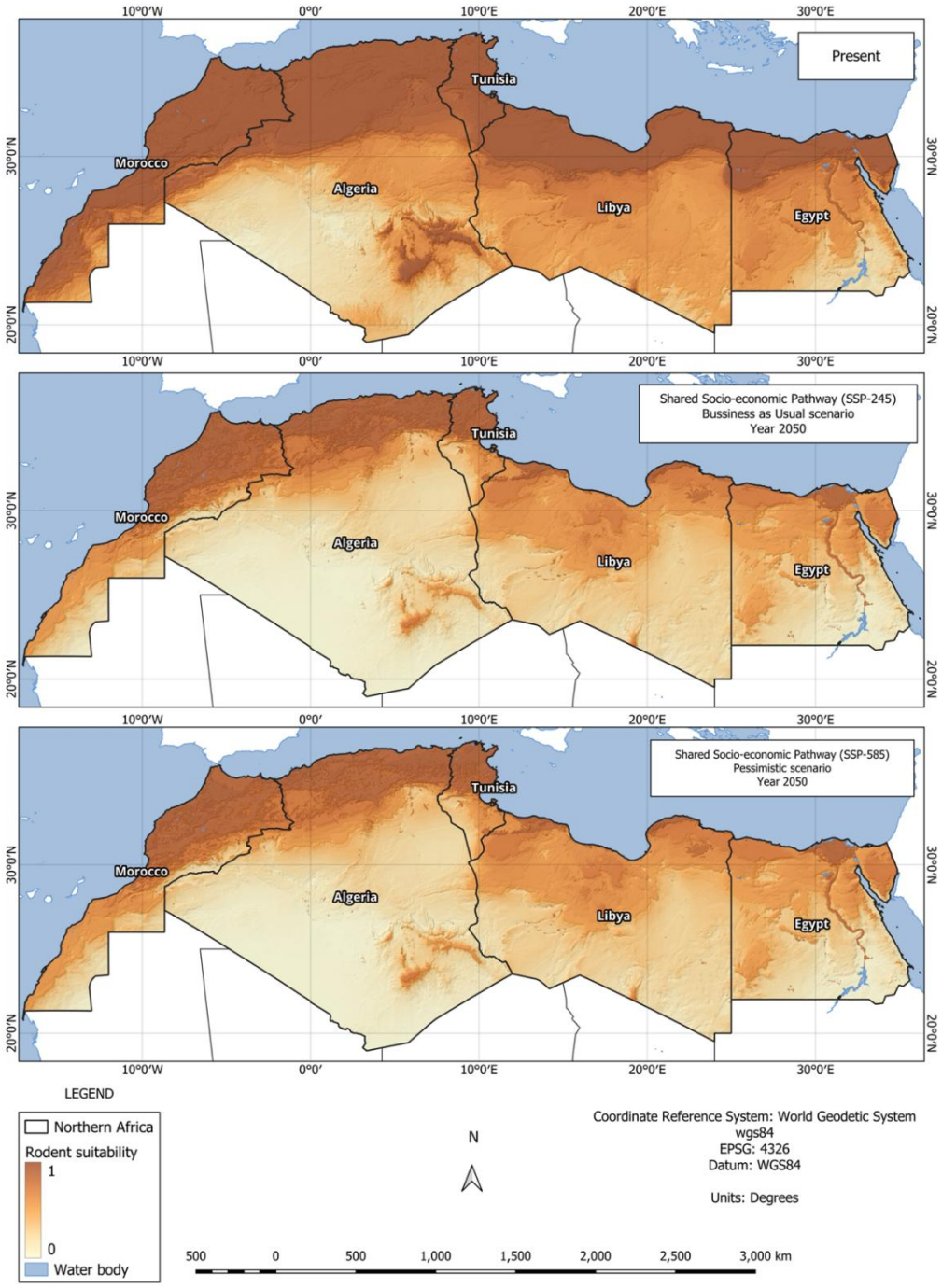

Figure C.1: Rodent suitability under the present and future. *Administrative boundaries were obtained from the Africa Countries dataset (ArcGIS Hub) and are licensed under the Esri Master License Agreement (https://hub.arcgis.com/datasets/africa::africa-countries/about). All raster layers were projected in WGS84 (EPSG:4326)*

Supplementary Material D: Model skill

Table D.1:.Model accuarcy

method	quarter	AUC_PR_mean	AUC_PR_sd	AUC_PR_CI_l	AUC_PR_CI_u	TSS_mean	TSS_CI_l	TSS_CI_u	pROC_mean	pROC_CI_l	pROC_CI_u	Cal_slope_mean	Boyce	Boyce_status	Score
additive_10	Q3	0.650377183339205	0.101565791328011	0.561352477888705	0.739401888789704	0.569079776661273	0.483760961265296	0.654398592057251	3.74532532279308	3.11209689051512	4.37855375507105	2.34430588839456	0.767	OK	1.2997564565587 1
additive_20	Q3	0.598184086820753	0.105840616946128	0.505412400358 94	0.690955773282567	0.518667644203408	0.424607474948918	0.612727813457899	3.01725985572805	2.08061907888611	3.95390063256998	1.94082364003619	0.703	OK	1.1080223173504 4
harmonic	Q3	0.525127335578066	0.110024754357094	0.428688158362672	0.621566512793461	0.353883513473288	0.252139391265866	0.455627635680709	2.53337749938013	1.82476474028023	3.24199025848004	0.82864980673 6883	0.687	OK	0.9572776696862 98
additive_30	Q3	0.526400153404238	0.127861580376847	0.414326596130188	0.638473710678289	0.411000151980392	0.320289373534002	0.501710930426782	1.82229223036002	1.23746078560548	2.40712367511456	1.51604003419505	0.914	OK	0.9175385071489 3
additive_10	Q2	0.536079460264214	0.144156147268374	0.409723347820807	0.662435572707621	0.409301012945076	0.358788316036376	0.459813709853775	2.76079337495339	0.74821998612 2088	4.77336676378 47	1.42011201145153	0.214	OK	0.8268347696325 37
geometric	Q3	0.486916874215129	0.124044630111712	0.378188959884729	0.595644788545529	0.326752166387979	0.227148097108 16	0.426356235667797	1.69753259172834	1.05377362518965	2.34129155826702	0.68717598332 7289	0.677	OK	0.7730403264662 89
additive_20	Q2	0.502082413550194	0.137486491003501	0.381572405160846	0.622592421939542	0.347250092144925	0.305674061768 21	0.388826122521 64	2.38212992016303	1.34278686460217	3.42147297572 39	1.21358973389317	0.237	OK	0.7410924851716 31
additive_30	Q2	0.485665587618684	0.121217388803545	0.379415814022541	0.591915361214827	0.292035617329113	0.245129986151766	0.338941248506461	2.57525972273497	1.39451821489103	3.75600123057892	0.68017815904 5318	0.09	OK	0.7065921855365 54
additive_40	Q3	0.493265520104124	0.135144519354878	0.374808302654186	0.611722737554062	0.370790146638104	0.282544693042774	0.459035600233433	1.59614496301888	0.78561340749 3038	2.40667651854472	1.16519202651397	0.492	OK	0.6888401259522 21
additive_50	Q3	0.472092547547338	0.136153942351807	0.352750548087614	0.591434547007061	0.303711210124015	0.228960208598372	0.378462211649658	1.38100847096 23	0.65818334095231 8	2.10383360097229	0.84762780025 7896	0.476	OK	0.6217624457267 32
multiplicative	Q3	0.417425787277 37	0.103323701951 21	0.326860233541318	0.507991341013422	0.174747043773004	0.109796557230355	0.239697530315654	1.46383798057 79	0.93093320404233 2	1.99674275711347	0.32101746307 1702	0.442	OK	0.5880021623256 55
additive_70	Q3	0.445760156895123	0.133138528214359	0.329061235896046	0.562459077894199	0.253669762800341	0.215423964384166	0.291915561216515	1.39341117736 91	0.54166590883 2692	2.24515644590 551	0.47591595082 3066	0.347	OK	0.5573682194129 13

additive_60	Q3	0.456123347296565	0.135228729307593	0.337592317924931	0.574654376668199	0.273046846534058	0.228500057300292	0.317593635767824	1.44564738542283	0.593805212635949	2.29748955820971	0.630116939916659	0.294	OK	0.552563515850691
additive_40	Q2	0.446727160005112	0.118554169811703	0.342811757885811	0.550642562124414	0.181770112769258	0.107767323971247	0.255772901567269	2.63207454185327	0.943043623997218	4.32110545970932	0.019832681348 9334	-0.454	OK	0.470514362925528
additive_90	Q3	0.434648821805954	0.133270904492884	0.317833870014913	0.551463773596996	0.223777349950993	0.174604362667224	0.272950337234763	1.31834415584508	0.455126502001894	2.18156180968827	0.308100739725125	0.177	OK	0.466154065520406
additive_80	Q3	0.438249152785141	0.132910019864443	0.321750524505475	0.554747781064806	0.233123208183554	0.190828651640629	0.275417764726479	1.33089868762405	0.474653802926 95	2.18714357232114	0.367816624279 5	0.1	OK	0.440454209718548
geometric	Q2	0.353617648792447	0.105431505394 12	0.261204557827579	0.446030739757314	0.098151527048 7812	0.012218139033 4398	0.184084915064123	1.70531200041566	0.421121753063632	2.98950224776769	-0.553147865651 38	-0.058	OK	0.408216235251378
harmonic	Q2	0.347653177514415	0.102488833844395	0.257819404492394	0.437486950536435	0.090419613718 7381	0.012504750846 9616	0.168334476590515	1.71543843440087	0.517995361346458	2.91288150745529	-0.680228462090967	-0.152	OK	0.369902245126806
multiplicative	Q2	0.327688984845513	0.098868366947 4424	0.241028632666083	0.414349337024943	0.075879277610 9989	0.009797355690 4548	0.141961199531543	1.49839381204199	0.391209781914474	2.60557784216951	-1.645482199547 01	-0.167	OK	0.313592414899701
additive_50	Q2	0.379309434703085	0.109384534553781	0.283431424576218	0.475187444829952	0.125955323333895	0.044405976542 9911	0.2075046701248	1.85505432003117	0.472913832433398	3.23719480762894	-0.700762538580828	-0.609	OK	0.228463815613 63
additive_60	Q2	0.342117199480392	0.100445851852 5	0.254074146224 26	0.430160252736524	0.086269536101 6317	0.008401347696 6148	0.164137724506649	1.42759608241799	0.325528436263247	2.52966372857273	-1.308275308877 05	-0.639	OK	0.115596563600003
harmonic	Q4	0.226026762568341	0.064142066867 5956	0.169804795159723	0.282248729976959	0.002577260805 10889	-0.002474077551 67124	0.007628599161 88903	0.13770368492 0895	-0.070059750603 5799	0.34546712044537	-2.065588634276 82	0	OK	0.073261541658869
multiplicative	Q4	0.254685205972 07	0.058239374431 0209	0.203637081534201	0.305733330409939	0.001950912523 59973	-0.001872805759 64389	0.005774630806 84336	0.12109844098 1214	-0.047478000519 5197	0.28967488248 1948	-5.775800020656 63	-0.008	OK	0.072346911895 3769
additive_70	Q2	0.317766544423642	0.088073175159 9368	0.240568421175808	0.394964667671476	0.065687465545 3987	0.006346181659 83619	0.125028749430961	1.07226420753345	0.263971660719537	1.88055675434736	-1.544141388674 09	-0.56	OK	0.067143643500 4977

geometric	Q4	0.2547376604061460	0.0584542507579947	0.2035011920242480	0.3059741287888044	0.0010698552548 7731	-0.0010270225133 5313	0.0031667330231 0774	0.1098360427714 48	-0.0534472628377841	0.2731193483806 8	-2.2306382686624 3	-0.046	OK	0.0547287116864942
additive_80	Q2	0.3025966571184 91	0.0801639706059843	0.2323311299402 28	0.3728621842967755	0.0491833006195 03	0.0026870089272 423	0.0956795923117 636	0.9105940937477 39	0.2461590887014 01	1.5750290987940 8	-1.5969665209518 8	-0.553	OK	0.0312748102971467
additive_10	Q4	0.3334709259874 35	0.0927222338612804	0.2521977979954 1	0.4147440539794 6	0.0697685923269 177	-0.0050090222854 3008	0.1445462069392 66	0.6781090397447 1	-0.3956014136350 29	1.7518194931244 5	-0.8172573359366 54	-0.468	OK	0.0290697116118126
additive_80	Q1	0.2493240667354 69	0.0640660708160703	0.1931687115790 08	0.3054794218919 3	0	0	0	0.0788527127037899	-0.0130097939849238	0.1707152193925 04	-7.4534474572590 2	-0.143	OK	0.0084353558878 5176
additive_90	Q2	0.2882934750762 67	0.0785773541238947	0.2194186530078 05	0.3571682971447 29	0.0329305595705 124	0.0035261752073 9041	0.0623349439336 344	0.7785942113806 04	0.2044920555839 6	1.3526963671772 5	-1.5807319997342 5	-0.616	OK	-0.0264363507945233
additive_20	Q4	0.3207893399399 3	0.0896871537268 58	0.2421765280981 82	0.3994021517816 78	0.0550297388237 33	-0.0030687137341 7728	0.1131281913816 43	0.6272855279252 97	-0.3787932053689 31	1.6333642612195 3	-1.0805507259335	-0.596	OK	-0.0377790786622 08
additive_10	Q1	0.2495061872388 49	0.0641996066891332	0.1932337848796 72	0.3057785895980025	0	0	0	0.0925151457621195	-0.0186169298886969	0.2036472214129 36	-1.8047501918767 7	-0.317	OK	-0.0583957333998064
additive_20	Q1	0.2493855833769 3	0.0640182311766855	0.1932721607427 23	0.3054990060111138	0	0	0	0.0809360460371232	-0.0129084124665786	0.1747805045408 25	-2.0240417743187	-0.317	OK	-0.0607356741171893
additive_30	Q1	0.2493855833769 3	0.0640182311766855	0.1932721607427 23	0.3054990060111138	0	0	0	0.0809360460371232	-0.0129084124665786	0.1747805045408 25	-2.3039668889220 5	-0.317	OK	-0.0607356741171893
additive_40	Q1	0.2493855833769 3	0.0640182311766855	0.1932721607427 23	0.3054990060111138	0	0	0	0.0809360460371232	-0.0129084124665786	0.1747805045408 25	-2.6736904394412 6	-0.317	OK	-0.0607356741171893
additive_50	Q1	0.2493240667354 69	0.0640660708160703	0.1931687115790 08	0.3054794218919 3	0	0	0	0.0788527127037899	-0.0130097939849238	0.1707152193925 04	-3.1846376804339 4	-0.317	OK	-0.0611646441121482

additive_60	Q1	0.2493240667354690	0.0640660708160703	0.1931687115790080	0.3054794218931930	0	0	0	0.0788527127037899	-0.0130097939849238	0.1707152193925040	-3.9367162537871	-0.317	OK	-0.0611646441121482
additive_30	Q4	0.3036130594362720	0.0818322311337030	0.2318852643019090	0.3753408545700635	0.0372298946226608	-0.0112810619864439	0.0857408512317654	0.4883811114028950	-0.3031402990152280	1.2799025218210200	-1.4536025589000600	-0.629	OK	-0.0857551869076345
additive_40	Q4	0.2824246207199660	0.0698354458416399	0.2212122783085530	0.3436369631313780	0.0327931535696433	-0.0148308149629006	0.0804171221021872	0.3990888483086930	-0.2350626418686890	1.0332403384860700	-1.9241911628519700	-0.607	OK	-0.0999386754803396
additive_70	Q1	0.2493240667354690	0.0640660708160703	0.1931687115790080	0.3054794218931930	0	0	0	0.0788527127037899	-0.0130097939849238	0.1707152193925040	-5.1529782872356100	-0.548	OK	-0.1535646441121480
additive_60	Q4	0.2615042167376160	0.0603832215152570	0.2085769620068650	0.3144314714683680	0.0153353262009065	-0.0050562993074924 2	0.0357269517094223	0.1312094890032990	-0.0436756818058608	0.3060946598124580	-2.9603710049995800	-0.636	OK	-0.1727901936116240
additive_90	Q1	0.2493240667354690	0.0640660708160703	0.1931687115790080	0.3054794218931930	0	0	0	0.0788527127037899	-0.0130097939849238	0.1707152193925040	-13.451258671468900	-0.6	OK	-0.1743646441121480
additive_50	Q4	0.2702692267511770	0.0643933221903275	0.2138270283887450	0.3267114251136090	0.0279410441743057	-0.0146357517571368	0.0705178401058507	0.2161557378301180	-0.1005034623109900	0.5328149379712250	-2.4712688553796800	-0.714	OK	-0.1827267982488700
additive_90	Q4	0.2477063752926810	0.0595960045919529	0.1954691339395290	0.2999436166458330	0.0042164883574575 4	-0.0040476769643916 8	0.0124806536793068	0.0207127271770907	-0.0155600463167893	0.0569855006709708	-3.5153985596899900	-0.691	OK	-0.2218728818345540
additive_80	Q4	0.2500279024733690	0.0591980132710262	0.1981395094839630	0.3019162954627775	0.0048353262009649 6	-0.0046417390064292 4	0.0143123914083592	0.0603052529696628	-0.0491310294337395	0.1697415353730650	-3.6119873311907500	-0.784	OK	-0.2505663036712010
additive_70	Q4	0.2522303037413610	0.0598941385904264	0.1997317412184350	0.3047288662642870	0.0048353262009649 6	-0.0046417390064292 4	0.0143123914083592	0.0343377076286884	-0.0137642488766190	0.0824396641339959	-3.4476646953346900	-0.896	OK	-0.3001193324857970
geometric	Q1	0.3615745103765400	0.0745338393175174	0.2962439201790230	0.4269051005740570	0	0	0	0	0	0	NA	NA	too many zeros; drop_zeros=TRUE	NA

harmonic	Q1	0.088267615960 3462	0.073976992260 5147	0.015771495702 7426	0.16076373621 795	0	0	0	0	0	0	NA	NA	too many zeros; drop_zeros=TRUE	NA
multiplicative	Q1	0.361574510376 54	0.074533839317 5174	0.296243920179 023	0.42690510057 4057	0	0	0	0	0	0	NA	NA	too many zeros; drop_zeros=TRUE	NA

References

Benkova I, Volf P. Effect of temperature on metabolism of Phlebotomus papatasi (Diptera: Psychodidae). J Med Entomol. 2007 Jan;44(1):150-4. doi: 10.1603/0022-2585(2007)44[150:eotomo]2.0.co;2. PMID: 17294933.

Didan, K. (2021). *MODIS/Terra Vegetation Indices 16-Day L3 Global 1km SIN Grid V061* [Data set]. NASA Land Processes Distributed Active Archive Center. https://doi.org/10.5067/MODIS/MOD13A2.061 Date Accessed: 2026-05-06.

Hengl T, Heuvelink GBM, Kempen B, Leenaars JGB, Walsh MG, et al. (2015) Mapping Soil Properties of Africa at 250 m Resolution: Random Forests Significantly Improve Current Predictions. PLOS ONE 10(6): e0125814. https://doi.org/10.1371/journal.pone.0125814.

Lawyer PG, Ngumbi PM, Anjili CO, Odongo SO, Mebrahtu YB, Githure JI, Koech DK, Roberts CR. Development of Leishmania major in Phlebotomus duboscqi and Sergentomyia schwetzi (Diptera: Psychodidae). Am J Trop Med Hyg. 1990 Jul;43(1):31-43. doi: 10.4269/ajtmh.1990.43.31. PMID: 2382763.

Naimi, B. and Araújo, M.B. (2016), sdm: a reproducible and extensible R platform for species distribution modelling. Ecography, 39: 368-375. https://doi.org/10.1111/ecog.01881.

Parkash V, Ashwin H, Sadlova J, Vojtkova B, Jones G, Martin N, Greensted E, Allgar V, Kamhawi S, Valenzuela JG, Layton AM, Jaffe CL, Volf P, Kaye PM, Lacey CJN. A clinical study to optimise a sand fly biting protocol for use in a controlled human infection model of cutaneous leishmaniasis (the FLYBITE study). Wellcome Open Res. 2021 Jun 30;6:168. doi: 10.12688/wellcomeopenres.16870.1. PMID: 34693027; PMCID: PMC8506224.

Zomer, R.J., Xu, J. & Trabucco, A. Version 3 of the Global Aridity Index and Potential Evapotranspiration Database. *Sci Data* **9**, 409 (2022). https://doi.org/10.1038/s41597-022-01493-1.